© 2017. Published by The Company of Biologists Ltd | Development (2017) 144, 2153-2164 doi:10.1242/dev.150763

RESEARCH ARTICLE

Apical constriction is driven by a pulsatile apical myosin network in delaminating *Drosophila* neuroblasts

Yanru An[1,2], Guosheng Xue[1], Yang Shaobo[1,2], Deng Mingxi[1,2], Xiaowei Zhou[3], Weichuan Yu[3], Toyotaka Ishibashi[1], Lei Zhang[4,5,*] and Yan Yan[1,2,*]

ABSTRACT

Cell delamination is a conserved morphogenetic process important for the generation of cell diversity and maintenance of tissue homeostasis. Here, we used *Drosophila* embryonic neuroblasts as a model to study the apical constriction process during cell delamination. We observe dynamic myosin signals both around the cell adherens junctions and underneath the cell apical surface in the neuroectoderm. On the cell apical cortex, the nonjunctional myosin forms flows and pulses, which are termed medial myosin pulses. Quantitative differences in medial myosin pulse intensity and frequency are crucial to distinguish delaminating neuroblasts from their neighbors. Inhibition of medial myosin pulses blocks delamination. The fate of a neuroblast is set apart from that of its neighbors by Notch signaling-mediated lateral inhibition. When we inhibit Notch signaling activity in the embryo, we observe that small clusters of cells undergo apical constriction and display an abnormal apical myosin pattern. Together, these results demonstrate that a contractile actomyosin network across the apical cell surface is organized to drive apical constriction in delaminating neuroblasts.

KEY WORDS: Apical constriction, *Drosophila* neuroblast, Myosin

INTRODUCTION

The movement of single cells out of an epithelial layer is important for the generation of diverse cell types during organogenesis. For example, single cells moving into the interior of the sea urchin blastula give rise to the primary mesenchymal cells; and individual cells delaminating from the neural tube in vertebrates give rise to a variety of cell types, such as peripheral neurons and glia. In adult epithelial tissues, extrusions of single cells have been shown to counterbalance growth (Eisenhoffer et al., 2012; Marinari et al., 2012). Single cells leaving an epithelium can adopt either of two fates. The first fate is to differentiate and generate other cell types, such as the primary mesenchymal cells derived from the sea urchin blastula and the neural crest cells that delaminate from the vertebrate neural tube. The second is to undergo apoptosis or anoikis after leaving the epithelial layer; this is the default fate for apoptotic cells extruded from the epithelial layer (Rosenblatt et al., 2001; Toyama et al., 2008) or for live cells extruded due to tissue crowding (Eisenhoffer et al., 2012; Marinari et al., 2012). Although the apoptotic single-cell extrusion process has been studied in several contexts (Gu and Rosenblatt, 2012), the nonapoptotic single-cell delamination process is less well characterized. It is unknown whether the molecular and cellular regulatory mechanisms for different types of single-cell extrusions are conserved. Moreover, it is unclear how cells experience internal and external force, change shape and move out of the epithelial layer without compromising epithelial integrity.

The *Drosophila* embryo has been established as an excellent system with which to study epithelial morphogenesis, including invagination and intercalation, because of its optical and genetic accessibility (Lecuit et al., 2011). Here, we developed *Drosophila* embryonic ventral nerve cord (VNC) neural stem cells (neuroblasts) as a model to study the mechanical processes of nonapoptotic single-cell delamination. Several hundred VNC neuroblasts delaminate from the embryonic ventral neuroectoderm region within 4 h of the onset of gastrulation (Campos-Ortega and Hartenstein, 1997). This highly predictable pattern allows us to track delamination processes with high spatiotemporal resolution. Delaminating neuroblasts undergo apical constriction as a first step in leaving the epithelial layer. The apical constriction process is primarily driven by an apical myosin network (Martin and Goldstein, 2014). However, the organization and dynamics of the actin-myosin network vary in different contexts (Martin and Goldstein, 2014). The contractile actin-myosin machinery important for apical constriction can be distinguished into two categories. First, the purse-string-like contraction of bundled actin-myosin fibers around the apical adherens junctions can generate force to drive apical constriction (Burgess, 1982). For example, when apoptotic cells are extruded from an MDCK cell monolayer, the actin-myosin ring is assembled in both the apoptotic cells and their neighbors during extrusion (Rosenblatt et al., 2001). Contraction of the actin-myosin ring assembled in the dying cells is important for the early stage of apical constriction in this system (Kuipers et al., 2014). Second, the actin-myosin meshwork underlying the apical plasma membrane has been shown to organize into cortical flows and pulses that drive apical constriction in several cell types. For example, in ventral furrow cells undergoing invagination as a group of cells in *Drosophila* embryos the myosin foci and fibers arise across the apical surface, move to the center of the cells, form large spots with high intensity and disperse. This nonjunctional myosin movement on the cell apical surface was termed medial myosin pulses, and each pulse coincides with a rapid apical area constriction phase (Martin et al., 2009; Mason et al., 2013). The amnioserosa cells also assemble a dynamic medial actomyosin network that drives apical cell shape fluctuations during the *Drosophila* dorsal closure process (Blanchard et al., 2010; David et al., 2010). Moreover, the salivary gland placode cells also

[1]Division of Life Science, Hong Kong University of Science and Technology, Clear Water Bay, Kowloon, Hong Kong, China. [2]Center of Systems Biology and Human Health, School of Science and Institute for Advanced Study, Hong Kong University of Science and Technology, Clear Water Bay, Kowloon, Hong Kong, China. [3]Department of Electronic and Computer Engineering, Hong Kong University of Science and Technology, Clear Water Bay, Kowloon, Hong Kong, China. [4]Beijing International Center for Mathematical Research, Peking University, Beijing, 100871, China. [5]Center for Quantitative Biology, Peking University, Beijing, 100871, China.

*Authors for correspondence (zhangl@math.pku.edu.cn; yany@ust.hk)

Y.Y., 0000-0002-3677-5006

Received 21 February 2017; Accepted 28 April 2017

Development (2017) 144, 2153-2164 doi:10.1242/dev.150763

undergo apical constriction driven by a medial actomyosin network in *Drosophila* embryos (Booth et al., 2014; Röper, 2012). In all of these contexts, the contraction of an actomyosin network across the epithelial apical surface is crucial for the apical constriction process for a group of cells.

In this study, we tracked and analyzed the highly dynamic apical myosin network in delaminating neuroblasts. Combining quantitative analysis, drug inhibition and genetic experiments, we demonstrate that the apical constriction process in delaminating neuroblasts is dependent on a pulsatile actin-myosin meshwork underlying the apical plasma membrane, unlike the cases reported for single cells extruded from epithelia destined for apoptosis (Eisenhoffer et al., 2012; Hogan et al., 2009; Rosenblatt et al., 2001). Both our experimental results and mathematical modeling suggest that quantitative differences in myosin pulse intensity and frequency are sufficient to generate different outcomes for delaminating neuroblasts and their neighbors. Overall, we demonstrate a role of fate-determining Notch signaling activity in the apical constriction process in delaminating neuroblasts.

RESULTS

Drosophila embryonic neuroblasts undergo apical constriction as single cells

Drosophila VNC neuroblasts are derived from the neurogenic region that bilaterally occupies the embryonic ventral-lateral surface (Campos-Ortega and Hartenstein, 1997). We used a membrane-mCherry transgenic line (Martin et al., 2010) to visualize the apical cell shape change in the neurogenic region. Before the ventral furrow closes, the epithelial cells are mostly hexagon-shaped and morphologically indistinguishable in the neurogenic region. As the ventral furrow closes and the germband extension process starts, the cells in the neurogenic region start to exhibit morphological heterogeneity (Irvine and Wieschaus, 1994). Within 10 min after the ventral furrow closes, we start to observe clusters of cells adopting a characteristic 'flower-like' structure, with one cell in the center decreasing its apical area while the apical areas of neighboring cells undergo fluctuations (Fig. 1A,B and Movie 1). The clusters of cells maintain the flower-like structure on the apical surface for another 15-30 min before the center cell drops out of the imaging plane. These center cells have previously been characterized as 'bottle-like' cells expressing the neuroblast marker Inscuteable (Fig. 1C), and later become the first wave of neuroblasts detectable beneath the surface epithelium at embryonic stage 8 (Doe, 1992; Kraut and Campos-Ortega, 1996). Therefore, the reduction in apical area of neuroblasts is one of the earliest steps of delamination, and can be tracked and analyzed starting immediately after the ventral furrow closes (Fig. 1A).

Using the ventral midline as the positional reference, we imaged six to eight rows of cells from the ventral midline and quantitatively tracked the change in apical area for these cells, including delaminating neuroblasts, which later become the first and second rows of neuroblasts from the ventral midline under the epithelial layer (Doe, 1992). A neuroblast is initially indistinguishable from its neighbors by apical shape or area. As a neuroblast initiates the delamination program, we start to see that its apical area steadily decreases while its neighboring cells maintain their apical area with fluctuations (Fig. 1D,E). The delaminating neuroblasts reduce their apical area at an average rate of 5 μm^2/min, a rate comparable to the apical area reduction rate of ventral furrow cells that undergo multicellular tissue invagination (Martin et al., 2009). Moreover, similar to ventral furrow cells, the delaminating neuroblasts also undergo pulses of rapid apical area constriction interrupted by phases of apical area stabilization (Fig. 1F,G). During the rapid constriction phase, the area constriction rate exceeds 10 μm^2/min. On average, a presumptive neuroblast undergoes ~4.6 pulses in 6 min, and reduces its area to 50% of its original value.

Overall, this quantitative analysis shows that the apical constriction behavior of individual neuroblasts is similar to that of ventral furrow cells (Martin et al., 2009), in spite of the fact that delaminating neuroblasts undergo apical constriction as single cells whereas ventral furrow cells undergo apical constriction as a group of cells.

A dynamic apical myosin network exists during the apical constriction process in delaminating neuroblasts

The similarity between the apical constriction behavior displayed in ventral furrow cells and delaminating neuroblasts prompted us to test whether an actin-myosin network exists to drive the apical constriction process in delaminating neuroblasts. By monitoring myosin dynamics in live embryos using a Myosin-GFP transgenic line [myosin regulatory light chain (Spaghetti squash, Sqh), fused to GFP] (Martin et al., 2009; Royou et al., 2002), we observed that dynamic myosin foci and fibers are present on the apical cell cortex across the embryo surface. Importantly, the myosin foci and fibers display pulsatile coalescence movements in delaminating neuroblasts similar to those observed in ventral furrow cells, which are defined as medial myosin pulses (Fig. 2A,B and Movie 2). It is noteworthy that a dynamic myosin signal is also present at adherens junctions in delaminating neuroblasts (Fig. 2A,B and Movie 2), unlike in ventral furrow cells, where myosin predominantly localizes to the apical cortex (Martin et al., 2009).

The role of medial myosin coalescence in driving apical constriction in ventral furrow cells was demonstrated through quantification of myosin intensity and correlation analysis of myosin intensity change rate with apical constriction rate (Martin et al., 2009). We applied this method to dissect the contribution of medial and junctional myosin to the apical constriction process in delaminating neuroblasts. The correlation analysis showed that the apical constriction rate correlates significantly with the medial myosin intensity change rate, rather than the junctional myosin intensity change rate (Fig. 2C,D and Fig. S1). Notably, in both delaminating neuroblasts and ventral furrow cells, the correlation analysis shows that the peak myosin intensity change rate and peak apical constriction rate occur simultaneously (Fig. S2A,C), whereas the peak total myosin change rate precedes the peak apical constriction rate by 6 s (Fig. S2B,D), indicating that the myosin-driven apical constriction behavior of delaminating neuroblasts and ventral furrow cells is similar.

The delaminating neuroblasts are surrounded by cells that do not undergo apical constriction and exhibit apical area fluctuation. In the nondelaminating neighboring cells, the medial and junctional myosin intensity also undergoes dynamic changes. Moreover, we also observed a correlation between the medial myosin intensity change rate and the cell area change rate in neighboring cells (Fig. 2E,F and Fig. S1). Both the medial and junctional myosin intensity exhibit similar dynamic changes in amplitude and frequency for cells immediately next to a delaminating neuroblast (1st degree neighbors) and those at least one cell away from a delaminating neuroblast (2nd degree neighbors) (Fig. S3).

To address how the dynamic apical myosin network is organized to generate different outcomes for delaminating neuroblasts and their neighboring cells, we compared the change in myosin intensity in delaminating cells and neighboring cells. First, we observed that delaminating neuroblasts display higher medial myosin intensity than do their neighboring cells (Fig. 2G-I), whereas junctional myosin

Development (2017) 144, 2153-2164 doi:10.1242/dev.150763

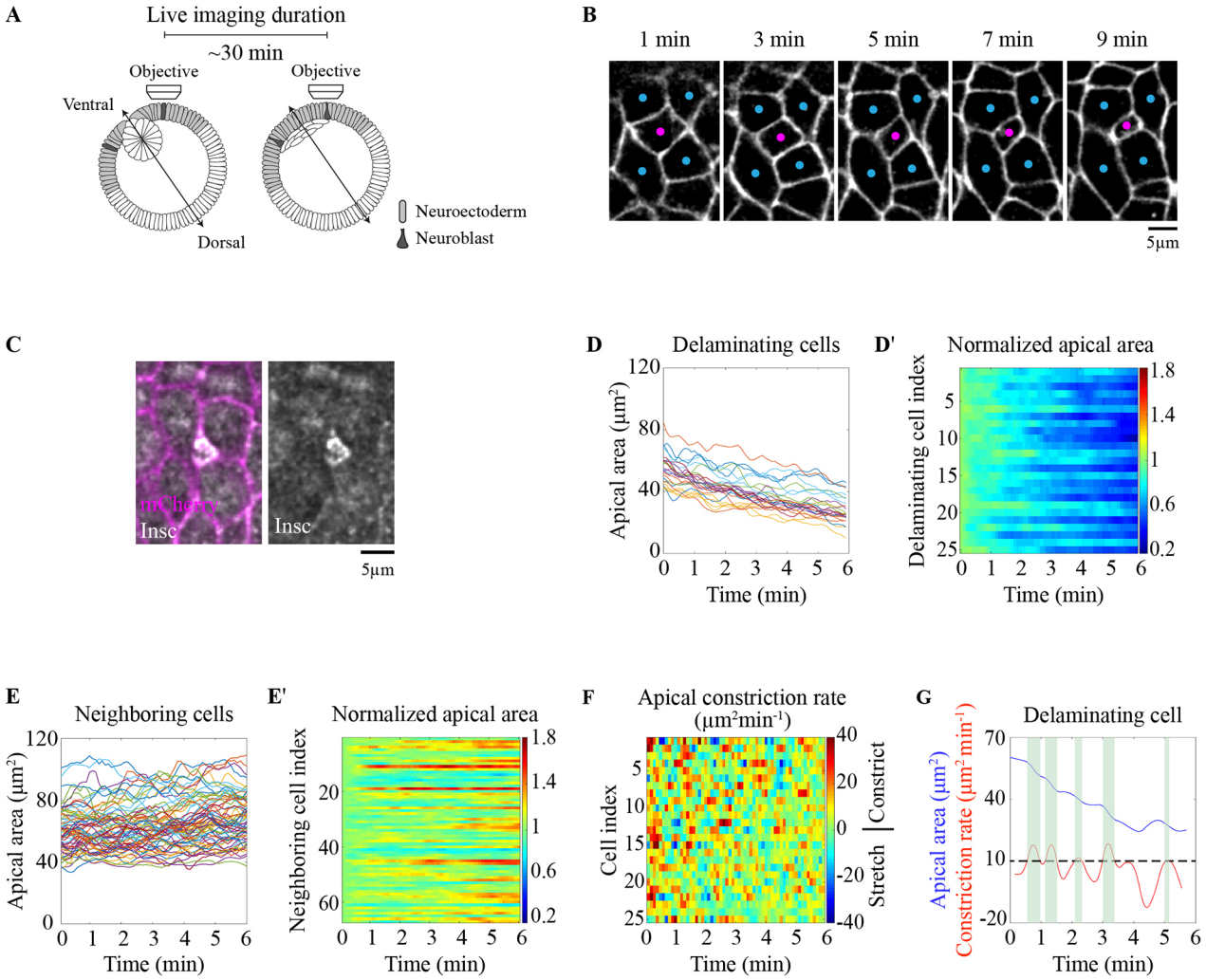

Fig. 1. *Drosophila* VNC neuroblasts undergo pulsatile apical constriction. (A) Schematic of embryo developmental stage and orientation for live imaging. The embryo was mounted with the ventrolateral neurogenic region facing the objective. Imaging was started as the ventral furrow closes. (B) Time-lapse images of the change in apical area of a neuroblast (magenta dot) and its surrounding cells (blue dots) in a representative cluster of cells (from Movie 2). The apical cell outline is visualized by membrane-mCherry. Scale bar: 5 µm. (C) A cluster of cells with a delaminating neuroblast in the center stained for Inscuteable (gray, n>50). The apical cell outline is visualized by membrane-mCherry (magenta). Scale bar: 5 µm. (D-E′) The apical area change (D,E) and normalized apical area change (D′,E′) in 25 neuroblasts (D,D′) and 67 neighboring cells (E,E′) during a 6-min delamination window from 12 embryos. In D′ and E′, at the imaging onset, the apical area of each cell is set as 1. For the subsequent time points, the apical area of each cell is shown as the original value divided by the cell area at imaging onset, highlighting the change in relative cell area over time for individual cells. Each row represents the normalized apical area for one cell over the 6-min time window. The normalized apical area at each time point for each individual cell is color coded, and the value varies between 0.2 and 1.8. (F) The apical area constriction rate of the 25 neuroblasts tracked in D. Each row represents the apical constriction rate for one cell over the 6-min time window. The apical constriction rate at each time point for each individual cell is color coded, and the value varies between −40 µm^2/min (stretch) and 40 µm^2/min (constriction). (G) Apical area (blue line) and constriction rate (red line) in a representative delaminating neuroblast.

intensity was not significantly different between the delaminating neuroblasts and their neighbors (Fig. 2K-M). Second, the medial myosin pulses appear at a higher frequency in delaminating neuroblasts (0.8 pulse/min) compared with in their neighboring cells (0.5 pulse/min) (Fig. 2J), whereas the junctional myosin pulses appear at a similar frequency in delaminating neuroblasts and their neighbors (0.5 pulse/min) (Fig. 2N). Together, these data raise the possibility that medial myosin pulses play an important role in driving apical constriction in delaminating neuroblasts.

Medial myosin pulses are required for the apical constriction process in delaminating neuroblasts

The formation of medial myosin pulses is dependent on a radial-polarized actin network with the pointed ends of actin filaments enriched in the medioapical region of ventral furrow cells (Coravos and Martin, 2016; Mason et al., 2013; Vasquez et al., 2014). Low-dose cytochalasin D (CytoD) treatment is a widely used method to disrupt the radial polarized apical actin network, and to block medial myosin pulses in ventral furrow cells (Coravos and Martin, 2016; Mason et al., 2013) and in cells undergoing shape deformation during *Drosophila* germband extension (Munjal et al., 2015).

To test the role of medial myosin pulses in the apical constriction process in delaminating neuroblasts, we injected the embryo with low-dose CytoD. Using a Utrophin-GFP strain to visualize the F-actin network (Rauzi et al., 2010), we observed that the apical actin meshwork, which also displays pulsatile coalescence movements, is disrupted by the low-dose CytoD treatment,

Development (2017) 144, 2153-2164 doi:10.1242/dev.150763

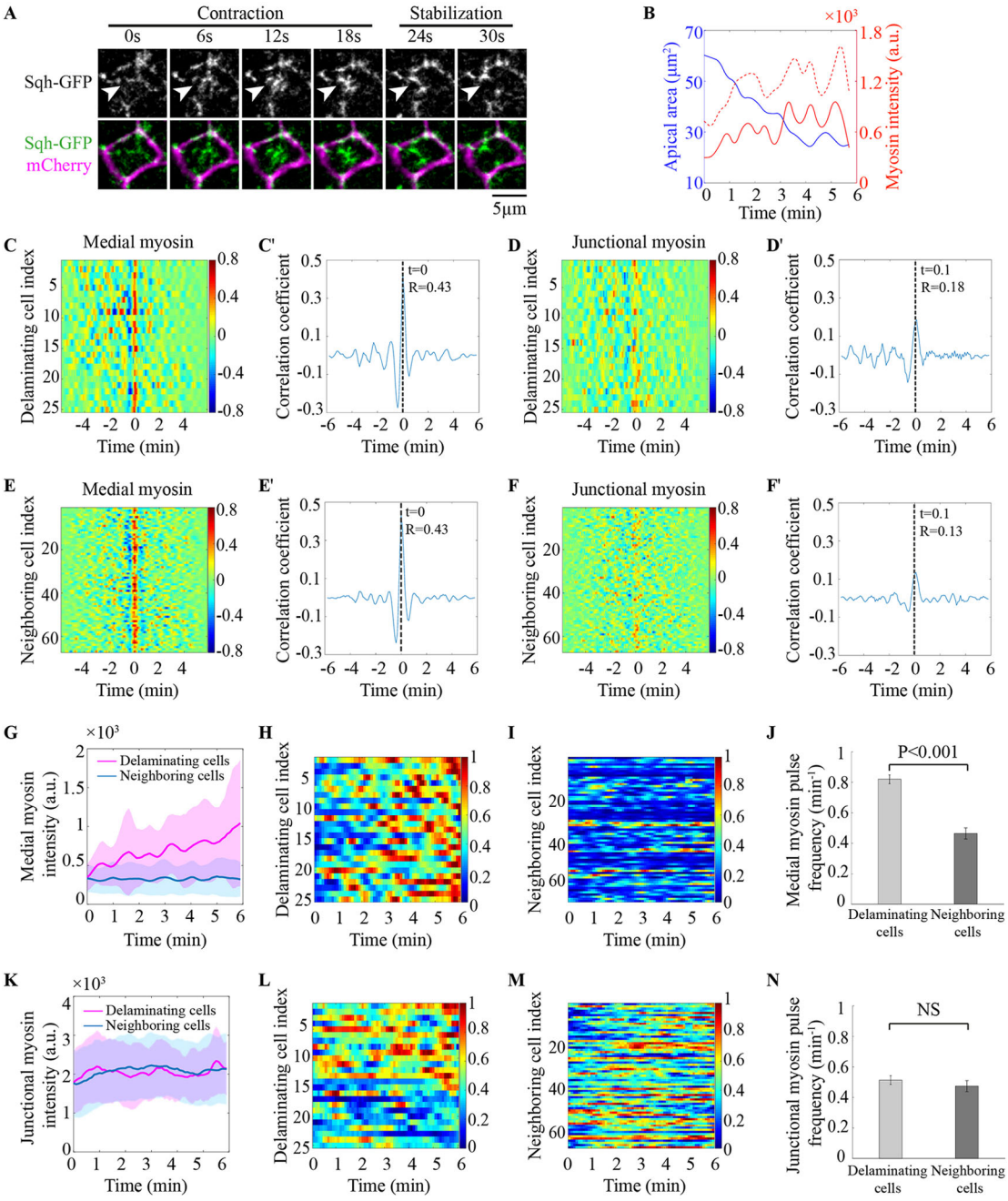

Fig. 2. A dynamic apical myosin network composed of medial and junctional myosin is present in delaminating neuroblasts and their neighboring cells. (A) Time-lapse images of a medial myosin pulse in a delaminating neuroblast from an embryo expressing Myosin (Sqh)-GFP (gray in top row, green in bottom row) and membrane-mCherry (magenta in bottom row). Arrowheads indicate that medial myosin foci coalesce and disassemble. Scale bar: 5 µm. (B) Plot of apical area (blue line), medial myosin intensity (red line) and junctional myosin intensity (dashed red line) as a function of time in a representative delaminating neuroblast. (C-F′) Plot of the correlation between apical constriction rate and myosin intensity change rate for individual delaminating neuroblasts (C-D′, *n*=25 from 12 embryos) and their neighboring cells (E-F′, *n*=67 from 12 embryos) against time offset for medial (C,E) and junctional (D,F) myosin. Mean cross-correlation against time offset for C,D,E,F is plotted in C′,D′,E,′F′. (G) Plot of mean medial myosin intensity for delaminating neuroblasts (magenta line, *n*=25 from 12 embryos) and their neighboring cells (blue line, *n*=67 from 12 embryos) as a function of time. The color-shaded regions represent the s.d. (H,I) Plot of normalized medial myosin intensity for individual delaminating neuroblasts (H, *n*=25 from 12 embryos) and their neighboring cells (I, *n*=67 from 12 embryos) as a function of time. To compare the myosin intensity for each delaminating neuroblast with that of its neighboring cells, the myosin intensity was normalized within each cluster of cells using the following method: the maximum myosin intensity value was set as 1, the minimum value was set as 0, and the intensity values were calculated proportionally between 0 and 1; each row represents the normalized medial myosin intensity (color coded) for one cell over a 6-min time window. (J) Quantification of medial myosin pulse frequency in delaminating neuroblasts (*n*=25 from 12 embryos) and their neighboring cells (*n*=67 from 12 embryos). Error bars are s.e.m. *P*-value is calculated by one-way ANOVA. (K) Mean junctional myosin intensity for delaminating neuroblasts (magenta line, *n*=25 from 12 embryos) and their neighboring cells (blue line, *n*=67 from 12 embryos) as a function of time. Error bars are s.d. (L,M) Normalized junctional myosin intensity for individual delaminating neuroblasts (L, *n*=25 from 12 embryos) and their neighboring cells (M, *n*=67 from 12 embryos) as a function of time. The normalization method is described in H,I. Each row represents the normalized junctional myosin intensity (color coded) for one cell over the 6-min time window. (N) Quantification of junctional myosin pulse frequency in delaminating neuroblasts (*n*=25 from 12 embryos) and their neighboring cells (*n*=67 from 12 embryos). Error bars are s.e.m. NS, not significant by one-way ANOVA.

Development (2017) 144, 2153-2164 doi:10.1242/dev.150763

whereas the junctional actin signal remains unaffected (Fig. 3A and Movies 3 and 4). Consequently, the low-dose CytoD disrupts the medial myosin pulses but does not appreciably lower the junctional myosin intensity (Fig. 3B,C and Movies 5 and 6). Disruption of medial myosin pulses by a low dose of CytoD leads to a global reduction in delaminating cells in the neuroectoderm region (Fig. 3D). Moreover, although DMSO mock-injected embryos display orderly rows of delaminated neuroblasts marked by Achaete below the surface epithelial layer 90 min after the onset of gastrulation, the embryos injected with a low dose of CytoD show few delaminated neuroblasts at the same stage (Fig. 3E).

RhoGEF2, a RhoA activator, is required to organize medial myosin pulses in ventral furrow cells (Mason et al., 2016) and cells in the ectoderm during *Drosophila* germband extension (Kerridge et al., 2016). In particular, it was reported that depletion of RhoGEF2 through RNAi leads to a specific reduction in medial myosin without affecting junctional myosin in epithelial cells located in the germband (Kerridge et al., 2016). The delaminating neuroblasts are located in the ectoderm undergoing germband extension. We therefore used *RhoGEF2* RNAi to examine its effects in neuroblast delamination. In *RhoGEF2 RNAi* embryos we observed a significant reduction in medial myosin intensity but not in junctional myosin intensity, consistent with published results (Fig. 3F-G′ and Movies 7 and 8). Consequently, we observed fewer cells undergoing delamination in *RhoGEF2 RNAi* embryos (Fig. 3H,I).

Taken together, these experiments suggest that medial myosin pulses are important for the apical constriction process in delaminating neuroblasts.

Mathematical modeling reveals that myosin pulse intensity and frequency are key parameters for neuroblasts to overcome an energy barrier for delamination

The dynamic medial and junctional myosin flows and pulses are qualitatively similar in both delaminating neuroblasts and their neighbors. To address whether the quantitative differences in medial myosin pulses observed in our experiments are sufficient to generate different outcomes for delaminating cells and their neighbors, we propose a phase-field model to simulate the dynamics of the neuroblast delamination process. The phase-field method has been successfully used in modeling single-cell events, such as cell membrane bending and cell migration (Du et al., 2004; Shao et al., 2012; Wang et al., 2017). Here, we extend this approach to study the morphodynamics of a multicellular system.

We chose six cells with the periodic boundary condition to model the delaminating neuroblast (the center cell in Fig. 4) and its neighboring cells. We first computed the minimum energy path to quantify the process of neuroblast delamination (Fig. 4A). Before the neuroblast delaminates, the initial state of six cells of equal shape is found to be a steady metastable state. When the neuroblast starts to delaminate, the system needs to overcome an energy barrier by passing through a transition state, and as the apical area of the delaminating cell decreases to zero, the system reaches a final stable state with five cells. Such a path indicates that the neuroblast requires a driving force in order to delaminate. We use stochastic periodic signaling to simulate the myosin pulses observed in the experiments as the driving force. Using the statistical data of normalized medial myosin intensity and frequency in Fig. 2H,I, our model is able to reproduce the dynamic change in apical area of delaminating cells (Fig. 4B,C and Movie 9). If we reduce the median myosin pulse frequency from 1 to 0.5 pulse/min, the apical area fluctuates periodically (Fig. 4D). Similarly, when the mean of the median myosin intensity is decreased by half, the apical area also shows oscillations, but the neuroblast cannot delaminate (Fig. 4E).

The mathematical model suggests that the quantitative differences in medial myosin pulse intensity and frequency are indeed sufficient to generate different outcomes for delaminating cells and their neighbors. Only a sufficiently high frequency and intensity median myosin pulse can drive the neuroblast to exceed the energy barrier in the minimum energy path and lead to delamination.

Perturbation of cell fate-determining Notch signaling activity leads to an abnormal delamination pattern in the neuroectoderm

Notch signaling activity is crucial for inhibiting neuroblast fate in the neighboring cells surrounding a chosen neuroblast (Campos-Ortega and Knust, 1990; Jan and Jan, 1994). During *Drosophila* early embryogenesis, the action of axis-patterning genes turns on the expression of proneural genes in clusters of cells in the neuroectoderm. Every cell in a proneural cluster has the potential to become a neuroblast. Through a lateral inhibition process mediated by Notch-Delta signaling activity, one cell from a proneural cluster is specified as a neuroblast, while the rest of the cells in the cluster that have higher Notch signaling activity remain epithelial cells. During the formation of proneuromast rosettes in the zebrafish posterior lateral line primordium, morphogenesis is independent of cell fate-determining Notch-Delta signaling activity (Hava et al., 2009). In *Drosophila* embryos, it has been shown that overexpression of the Notch intracellular domain (NICD) leads to premature cell division in the ventral neuroectoderm (Hartenstein et al., 1994). However, it remains unclear whether and how Notch signaling activity affects the cellular processes of neuroblast delamination including the apical constriction process.

To understand how differential Notch signaling activity in a proneural cluster affects the delamination process, in particular the apical constriction process, we lowered Notch signaling activity by injecting embryos with *Delta* or *Notch* dsRNA (Fig. S4). We observed that clusters of cells, which all adopt neuroblast fate, undergo apical constriction (Fig. 5A,C,D and Movies 10 and 11). Individual cells from a delaminating cluster still undergo pulses of apical constriction correlated with the dynamic change in medial myosin intensity (Fig. 5B,E,F and Fig. S5). In the *Delta RNAi* embryos, the delaminating neuroblasts exhibit higher medial myosin intensity than do the nondelaminating cells, whereas junctional myosin intensity in both delaminating cells and nondelaminating cells is similar (Fig. 5G,H). However, on average, these cells in the *Delta RNAi* embryos reduce their apical area at a rate of 2.5 μm^2/min, slower than the rate of delaminating neuroblasts in water-injected control embryos (Fig. 5I). The delaminating cells in *Delta RNAi* embryos exhibit a reduction in medial myosin pulse frequency from 0.8 to 0.5 pulse/min in comparison with controls, while the non-delaminating cells also exhibit a reduction in medial myosin pulse frequency from 0.5 to 0.2 pulse/min (Fig. 5J). When medial myosin pulse frequency is reduced in delaminating neuroblasts, we expect that three parameter changes can lead to effective apical constriction in *Delta RNAi* or *Notch RNAi* embryos: first, the overall energy barrier for neuroblast delamination is reduced; second, the medial myosin pulse intensity increases in delaminating neuroblasts; third, the apical constriction process can be driven by a compensatory mechanism such as an increase in junctional myosin contraction (Fig. S6). Quantitative analysis indicates that medial myosin intensity is higher in delaminating neuroblasts in *Delta RNAi* or *Notch RNAi* embryos, and that junctional myosin intensity is significantly higher in

Development (2017) 144, 2153-2164 doi:10.1242/dev.150763

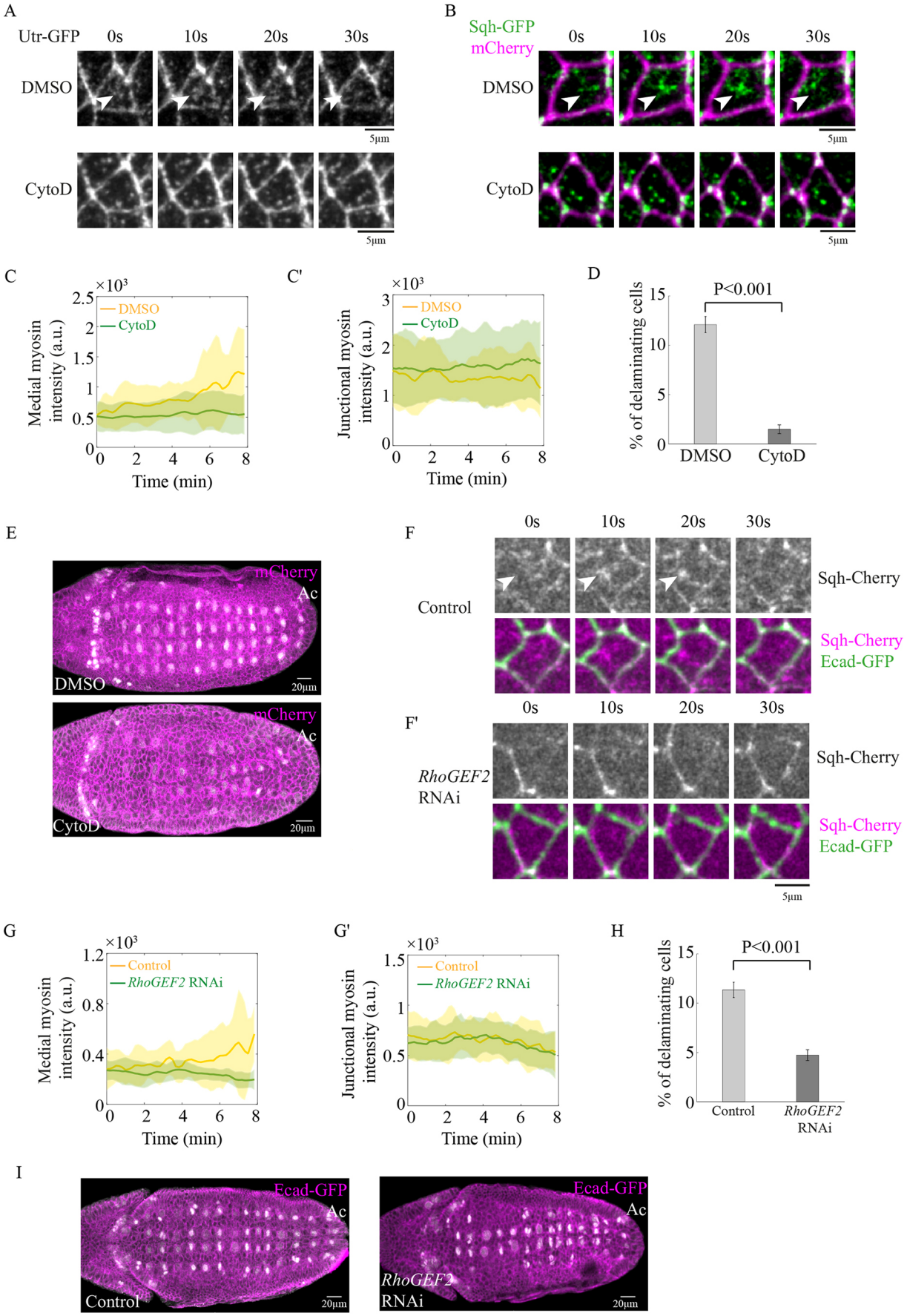

Fig. 3. See next page for legend.

Development (2017) 144, 2153-2164 doi:10.1242/dev.150763

Fig. 3. Medial myosin pulses promote apical constriction in delaminating neuroblasts. (A) Time-lapse images of apical F-actin visualized by Utrophin (Utr)-GFP in a presumptive neuroblast from a DMSO-injected embryo (top row) and an embryo injected with 0.25 mg/ml CytoD (bottom row). Note that in embryos injected with a low dose of CytoD, the medial actin forms discrete foci and fails to form a meshwork that coalesces and disassembles. Arrowheads indicate that the medial actin meshwork coalesces and disassembles. Scale bars: 5 µm. (B) Time-lapse images of apical myosin visualized by Myosin-GFP (green) in a presumptive neuroblast from a DMSO-injected embryo (top row) and an embryo injected with 0.25 mg/ml CytoD (bottom row). The apical cell outline is visualized by membrane-mCherry (magenta). Arrowheads indicate that the medial myosin foci coalesce and disassemble. Note that medial myosin pulses are depleted in embryos injected with low-dose CytoD. Scale bars: 5 µm. (C,C′) Mean medial myosin intensity (C) and mean junctional myosin intensity (C′) as a function of time in delaminating neuroblasts (yellow line, *n*=15) from five DMSO-injected embryos and presumptive neuroblasts (green line, *n*=47) from 15 embryos injected with 0.25 mg/ml CytoD. Error bars are s.d. (D) Quantification of the percentage of delaminating cells observed in DMSO-injected embryos (*n*=5) and embryos injected with 0.25 mg/ml CytoD (*n*=15) in a 10-min time window. Error bars are s.e.m. *P*-value is calculated by one-way ANOVA. (E) Embryos injected with DMSO and 0.25 mg/ml CytoD were stained for Achaete (gray) 90 min after the onset of gastrulation. The apical cell outline is visualized by membrane-mCherry (magenta). Scale bars: 20 µm. (F,F′) Time-lapse images of apical myosin visualized by Myosin-mCherry (gray in top row, magenta in bottom row) in a neuroblast from a control embryo (F) and a *RhoGEF2 RNAi* embryo (F′). The apical cell outline is visualized by E-cadherin (Ecad)-GFP (green). Arrowheads indicate that medial myosin foci coalesce and disassemble. Embryo genotypes are described in the legends of Movies 7 and 8. Scale bar: 5 µm. (G,G′) Plot of mean medial myosin intensity (G) and mean junctional myosin intensity (G′) as a function of time in delaminating neuroblasts (yellow line, *n*=13) from seven control embryos and presumptive neuroblasts (green line, *n*=21) from five *RhoGEF2 RNAi* embryos. Error bars are s.d. (H) Quantification of the percentage of delaminating cells observed in control embryos (*n*=8) and *RhoGEF2 RNAi* embryos (*n*=7) in a 10-min time window. Error bars are s.e.m. *P*-value is calculated by one-way ANOVA. (I) Control and *RhoGEF2 RNAi* embryos were stained for Achaete (gray) 90 min after the onset of gastrulation. The apical cell outline is visualized by E-cadherin-GFP (magenta). Scale bars: 20 µm.

delaminating neuroblasts in these embryos than in water-injected control embryos (Fig. 5K,L). On close examination of the myosin network, we noticed a strong accumulation of myosin fibers and cables around the junctional region in the delaminating cells in the *Delta RNAi* or *Notch RNAi* embryos (Fig. 5M and Movie 12), supporting the possibility that an increase in junctional myosin activity compensates partially for the reduction in medial myosin pulse frequency in these embryos.

DISCUSSION

The apical constriction process differs for delaminating cells destined for differentiation and extruding cells destined for apoptosis

Previous studies have shown that the formation of a junctional actin-myosin contractile ring is crucial for single cells destined for apoptosis to be extruded from epithelia (Eisenhoffer et al., 2012; Hogan et al., 2009; Rosenblatt et al., 2001). Here, we demonstrate that a pulsatile medial myosin network is required for delaminating neuroblasts leaving the epithelia. It is possible that the type of myosin contractility (medial versus junctional) adapted to promote the departure of single cells from epithelia is cell type specific. For cells leaving the epithelia for differentiation, our results support that the apical constriction process is primarily cell-autonomous and largely relies on the medial myosin network within the cell. For cells being extruded from the epithelia due to tissue crowding or apoptosis, the apical area reduction process is likely to be triggered by the neighboring cells and relies on the assembly of a junctional actin-myosin ring. It will be interesting to examine whether the two types of actin-myosin organization can be categorized as being associated with the cell-autonomous or the passive squeezing mode of departure through studying further types of apical constriction processes during development.

A few differences distinguish the otherwise largely similar apical constriction processes of delaminating neuroblasts and ventral furrow cells

The apical constriction process in ventral furrow cells during invagination is well characterized (Martin and Goldstein, 2014). The delaminating neuroblasts display similarity with ventral furrow cells in terms of apical constriction speed, duration, pulsatile behavior and the underlying actin-myosin network organizational mode. In both cell types, a pulsatile medial myosin network is crucial for the apical constriction process. However, a few differences exist between the two cell types.

Intense and dynamic myosin signals can be detected in the junctional region of delaminating neuroblasts, but not in the junctional region of ventral furrow cells. The delaminating neuroblasts reside in the elongating germband and the junctional myosin undergoes dynamic rearrangements to drive cell-cell intercalation during germband extension (Bertet et al., 2004; Irvine and Wieschaus, 1994). Although the correlation coefficient between junctional myosin change rate and apical constriction rate in delaminating neuroblasts is low, it does not exclude the possibility that the junctional myosin might play a role in apical constriction. Our data do not exclude a model in which the feedback between medial and junctional myosin networks exists to drive the apical constriction process in delaminating neuroblasts.

Importantly, the upstream regulatory signals for ventral furrow cells and delaminating neuroblasts are different. Snail and Twist are two crucial regulators for the apical constriction process in ventral furrow cells (Martin et al., 2009). In delaminating neuroblasts, *snail* and *twist* RNAi does not affect the apical constriction process (Movies 13 and 14).

Although a dynamic actomyosin network is present across all cells in the neuroectoderm, the delaminating neuroblasts and their neighbors differ in medial myosin pulse intensity and frequency. The fate of a neuroblast is set to be distinct from that of its neighbors by a lateral inhibition process mediated by the Notch-Delta signaling pathway. It is unclear how the fate-determining Notch signaling activity is translated into a patterned and dynamic myosin network in the neuroectoderm. The canonical Notch signaling pathway is dependent on enzymatic cleavage and the release of NICD, which translocates into the nucleus and functions as a transcriptional regulator. The uncleaved Notch also has an NICD-independent noncanonical function of binding to β-catenin and modulating β-catenin levels and activity (Andersen et al., 2012; Hayward et al., 2005). Since β-catenin is an important cytoskeletal regulator, as a first step we examined whether the apical constriction process of delaminating neuroblasts is dependent on NICD-mediated transcription. We injected the embryos with a widely used γ-secretase inhibitor, *N*-(*N*-[3,5-difluorophenacetyl-l-alanyl])-*S*-phenylglycine t-butyl ester (DAPT), to inhibit Notch cleavage and the release of NICD (Geling et al., 2002; Vaccari et al., 2008). We observed that DAPT-injected embryos display phenotypes similar to those of *Delta RNAi* or *Notch RNAi* embryos (Movies 11 and 15), indicating that the normal delamination pattern is dependent on NICD release and the canonical Notch pathway. In the future, it will be interesting to explore the molecular links and feedback between differential Notch signaling activity and a patterned myosin network in the neuroectoderm through experimental and modeling approaches.

Development (2017) 144, 2153-2164 doi:10.1242/dev.150763

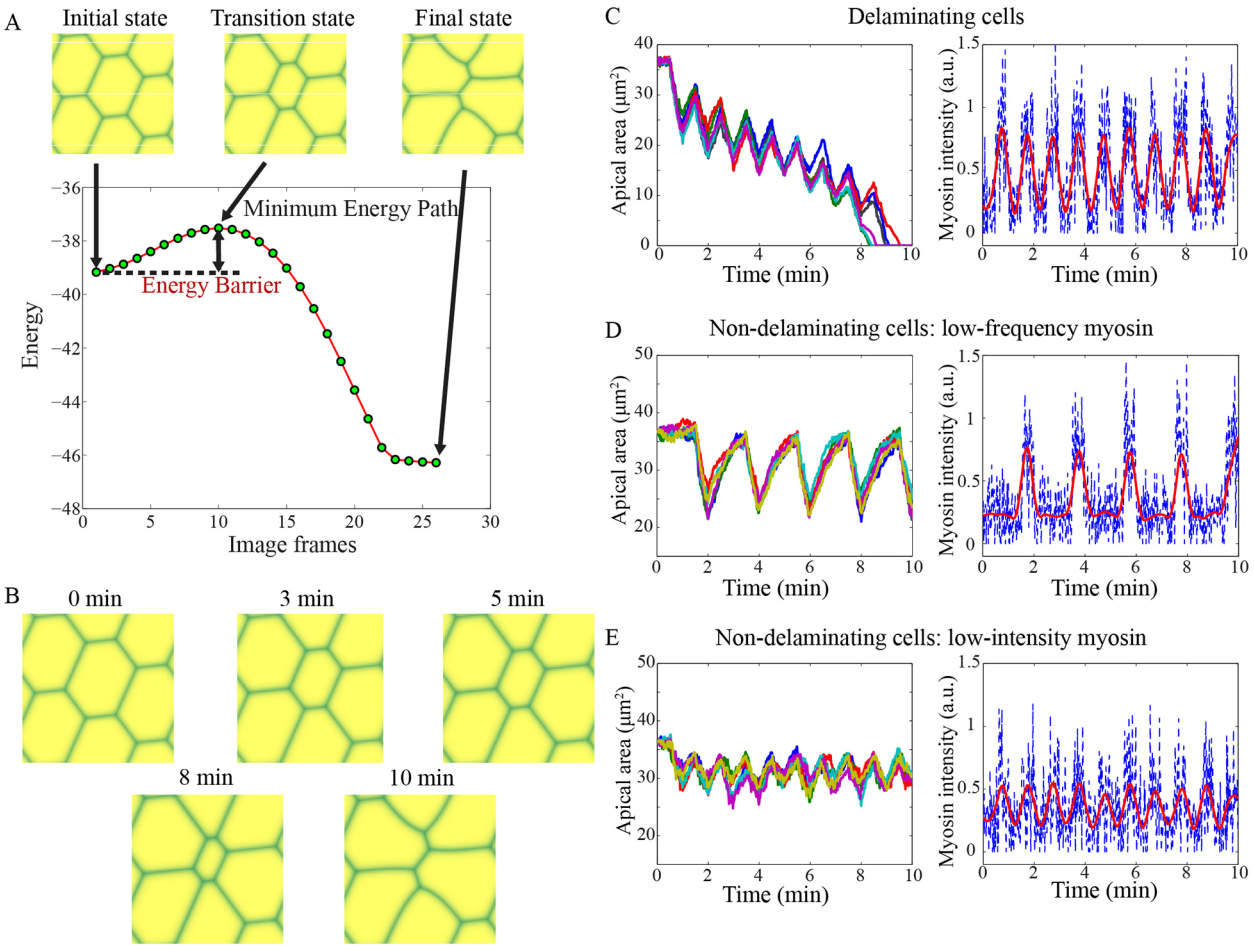

Fig. 4. Mathematical modeling of the neuroblast delamination process. (A) The minimum energy path reveals that the delaminating cell needs to overcome an energy barrier by passing through a transition state. (B) Time-lapse images of a cluster of cells with one cell in the center undergoing delamination in simulation. (C) Plots of apical area change as a function of time for delaminating cells from six simulations, and plots of the stochastic medial myosin intensity (blue dashed curve) and smooth medial myosin intensity (red solid curve) (mean, 0.5; frequency, 1 pulse/min). (D) Plots of apical area change and medial myosin intensity as a function of time for nondelaminating cells with low-frequency myosin (mean, 0.5; frequency, 0.5 pulse/min). (E) Plots of apical area change and medial myosin intensity as a function of time for nondelaminating cells with low-intensity myosin (mean, 0.25; frequency, 1 pulse/min).

MATERIALS AND METHODS

Fly stocks

The fluorescent protein fusion stock *sqh*^{P}-Sqh::GFP; *Gap43*::mCherry (Martin et al., 2010) was obtained from the Martin laboratory. Utrophin-GFP was obtained from the Lecuit laboratory (Rauzi et al., 2010). The *sqh*^{P}-Sqh::mCherry *mat67*-Gal4; *ubi*^{P}-ECad-GFP *mat15*-Gal4/TM3 line was obtained from the Wieschaus laboratory (Weng and Wieschaus, 2016). *RhoGEF2* RNAi (Bloomington, 34643) and TRiP background control line (Bloomington, 36303) were obtained from the Bloomington Drosophila Stock Center.

Immunofluorescence staining and western blotting

Embryos were fixed and stained according to standard protocols (Sullivan et al., 2000). The primary antibodies used were rabbit anti-Insc [1:1000, a gift from the Doe laboratory (Kraut and Campos-Ortega, 1996)] and mouse anti-Ac (1:20, Developmental Studies Hybridoma Bank). The secondary antibodies used were Alexa Fluor 405-conjugated goat anti-rabbit IgG (1:500, A-31556, Thermo Fisher) and Alexa Fluor 405-conjugated goat anti-mouse IgG (1:500, A-31553, Thermo Fisher). Antibodies used in western blotting are described in the supplementary Materials and Methods.

Fly embryo live imaging

Embryos of the correct stage were collected, dechorionated in bleach for 40 s, washed with double-distilled water and mounted with the ventrolateral side up on a slide coated with embryo glue (30 cm Scotch double-sided tape dissolved in 5 ml heptane). No. 1 coverslips (Marienfeld-Superior) were glued to the slide using double-sided tape as spacers. A No. 0 coverslip (Marienfeld-Superior) was then added on top of the spacers to create a chamber in which embryos would not be compressed. The chamber was filled with halocarbon oil 27 (Sigma, H8773).

All images were acquired on a Leica TCS SP8 confocal microscope at room temperature with a 40×/1.1 NA water-immersion objective. The pinhole was set at 1.5 Airy units. For two-color simultaneous excitation, a 488 nm OPSL laser (Coherent) was used to excite GFP and a 552 nm OPSL laser (Coherent) was used to excite mCherry. The band-pass filters for detection were set at 492-538 nm for GFP and 558-650 nm for mCherry. For wild-type, water-injected and *Delta RNAi* embryos, images were acquired at 6 s intervals for 30 min. For each time point, the images were taken as four *z*-slice stacks with a *z*-stack step size of 0.8 µm. For DMSO-injected, CytoD-injected, DAPT-injected, *RhoGEF2 RNAi* and TRiP line background control embryos, images were acquired at 10 s intervals for 50 min as seven *z*-slice stacks 0.8 µm apart.

Double-stranded RNA (dsRNA) synthesis

Primers for dsRNA synthesis are listed in the supplementary Materials and Methods. Genomic DNA was extracted from *sqh*^{P}-Sqh::GFP; *Gap43*::mCherry flies. PCR products were amplified from the genomic DNA. The PCR products were purified using a DNA Clean & Concentrator-5 kit (Zymo Research) and used as templates for *in vitro* transcription reaction using a MEGAscript transcription kit (Invitrogen Ambion). The dsRNA was

Development (2017) 144, 2153-2164 doi:10.1242/dev.150763

purified with an RNA Clean & Concentrator-5 kit (Zymo Research) and resuspended in diethyl pyrocarbonate (DEPC)-treated water.

Embryo drug injection and dsRNA injection

To prepare embryos for drug injection or dsRNA injection, embryos of the appropriate stage were dechorionated in bleach, washed in water and mounted on a glass slide with the ventrolateral side up. The embryos were then desiccated for 9 min and covered with halocarbon oil 700 (Sigma, H8898) for injection. The embryos were injected laterally at the posterior end. After injection, the halocarbon oil 700 was flushed away using halocarbon oil 27, and the injected embryos were covered with a thin layer of halocarbon oil 27. CytoD (Enzo Life Sciences) was resuspended at 5 mg/ml,

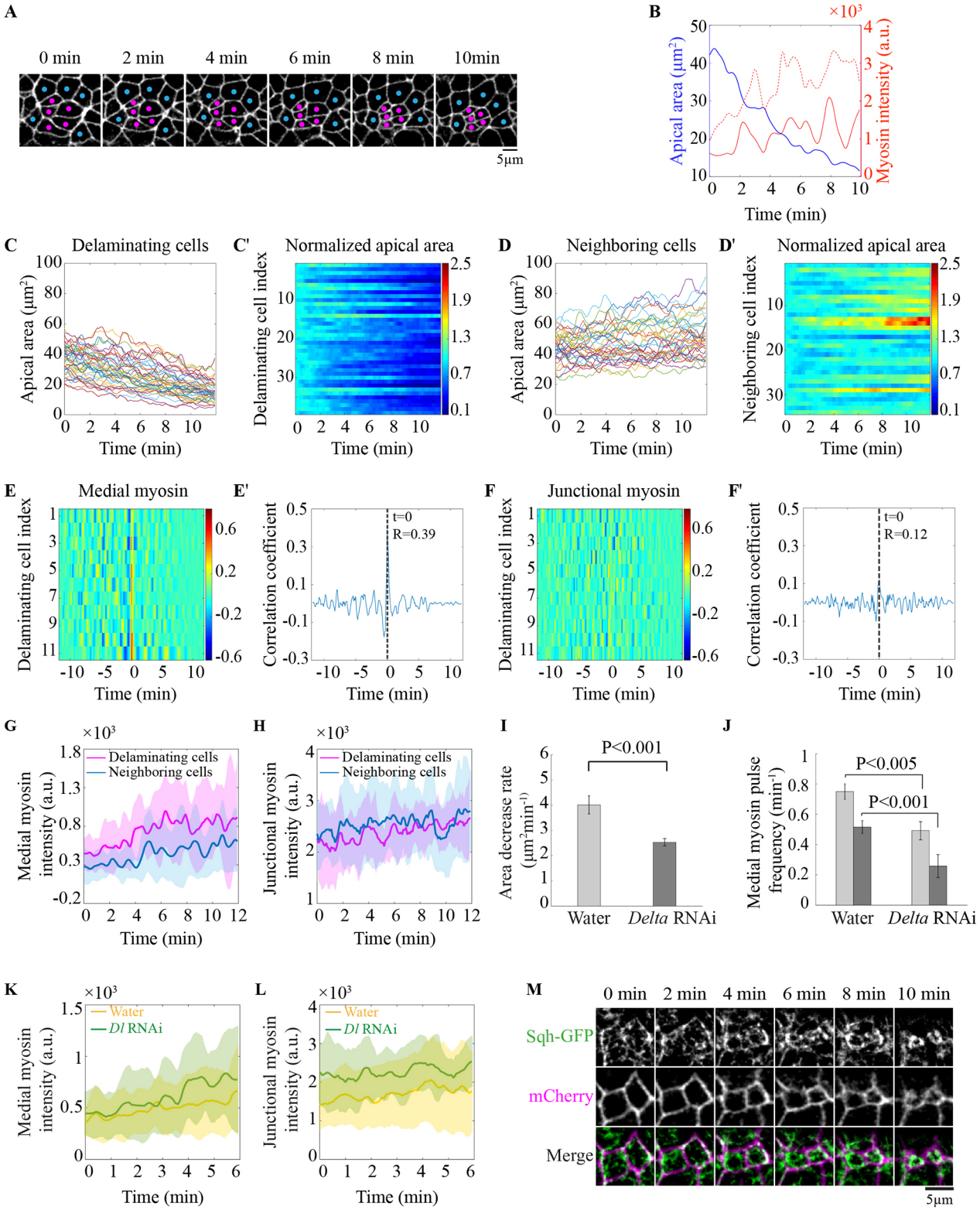

Fig. 5. See next page for legend.

Development (2017) 144, 2153-2164 doi:10.1242/dev.150763

Fig. 5. Small clusters of presumptive neuroblasts undergo apical constriction upon inhibition of Notch signaling activity. (A) Time-lapse images of the apical area visualized by membrane-mCherry in clusters of neuroblasts (magenta dots) and their surrounding cells (blue dots) from a *Delta RNAi* embryo. Scale bar: 5 µm. (B) Apical area (blue line), medial myosin intensity (red line) and junctional myosin intensity (dashed red line) as a function of time for a representative neuroblast from a *Delta RNAi* embryo. (C-D′) Change in apical area (C,D) and normalized apical area (C′,D′) in 39 neuroblasts (C,C′) and 34 neighboring cells (D,D′) from eight *Delta RNAi* embryos during a 12-min delamination window. In C′ and D′, at the imaging onset, the apical area of each cell is set as 1. For the subsequent points, the apical area of each cell is shown as the original value divided by the cell area at imaging onset, highlighting the change in relative cell area over time for an individual cell. Each row represents the normalized apical area for one cell over the 12-min time window. The normalized apical area at each time point for each individual cell is color coded, and the value varies between 0.1 and 2.5. (E-F′) Correlation between apical constriction rate and myosin intensity change rate for individual delaminating neuroblasts (n=11, from four *Delta RNAi* embryos) against time offset for medial myosin (E) and junctional myosin (F). Mean cross-correlation against time offset for E and F is plotted in E′ and F′. (G,H) Mean medial (G) and junctional (H) myosin intensity as a function of time for delaminating neuroblasts (magenta line, n=11, from four embryos) and their neighboring cells (blue line, n=10, from four embryos) in *Delta RNAi* embryos. Error bars are s.d. (I) Quantification of apical area decrease rate for delaminating neuroblasts in water-injected embryos (n=18, from eight embryos) and *Delta RNAi* embryos (n=39, from eight embryos). Error bars are s.e.m. P-value is calculated by one-way ANOVA. (J) Quantification of medial myosin pulse frequency for delaminating neuroblasts (n=18, from eight water-injected embryos; n=11, from four *Delta RNAi* embryos; light gray bar) and nondelaminating cells (n=52, from eight water-injected embryos; n=10, from four *Delta RNAi* embryos; dark gray bar). Error bars are s.e.m. P-value is calculated by one-way ANOVA. (K,L) Mean medial myosin intensity (K) and mean junctional myosin intensity (L) as a function of time in delaminating neuroblasts from eight water-injected embryos (yellow line, n=18) and four *Delta RNAi* embryos (green line, n=11). Error bars are s.d. (M) Time-lapse images of two delaminating neuroblasts from a *Delta RNAi* embryo expressing Myosin-GFP (gray in top row, green in bottom row) and membrane-mCherry (gray in middle row, magenta in bottom row). Note that Myosin-GFP forms intense cables around the junctional region that fail to dissemble over time. Scale bar: 5 µm.

diluted in DMSO and injected at 0.25 mg/ml, after ventral furrow closure immediately before imaging. DAPT (CAS208255-80-5, Santa Cruz Biotechnology) was kept as 30 mM stock in DMSO and injected at 10 mM within 30 min after egg laying. dsRNA was injected at 2-3 mg/ml within 30 min after egg laying. The injected embryos were then placed in a humid Petri dish at 25°C for ∼3 h prior to imaging.

Image processing and data analysis

The images were processed with the Fiji (Schindelin et al., 2012) and MATLAB (MathWorks). During image processing, the cell membrane outline is extracted from the bottom slice of the GAP43-mCherry or E-cadherin-GFP z-stack. Myosin-GFP or Myosin-mCherry signal represents the maximum-intensity z-projection of all slices from a z-stack. A Gaussian blur filter (radius=1 or 2 for myosin or membrane outline channel, respectively) was applied to reduce background noise. The Tissue Cell Segment Movie macro in Fiji was used to detect cell boundary and the junction width set as 1 µm.

Embryo Development Geometry Explorer (EDGE) (Gelbart et al., 2012) was used to measure total (myosinT) and medial (myosinM) myosin, total apical area (areaT) and cell perimeter (peri). Junctional myosin (myosinJ) was calculated by subtracting myosinM from myosinT. Medial (meanM) or junctional (meanJ) myosin intensity was calculated by dividing myosinM or myosinJ by its respective area. Junctional area (areaJ) equals the cell perimeter multiplied by 0.5 µm; medial area (areaM) equals areaT minus areaJ. Raw data at each time point were smoothed by averaging the values of three adjacent time points.

Apical constriction rate was calculated as the inverse value of the first derivative of apical area. The myosin intensity change rate was the first derivative of myosin intensity. Pearson cross-correlation between the apical constriction rate and myosin intensity change rate was calculated using the MATLAB toolbox for different time offsets. Cell area was normalized by setting the first frame value of each cell as 1; the data of subsequent frames were calculated proportionally (Figs 1 and 5). The myosin intensity was normalized so that the maximum value of all cells in each cluster was 1 and the minimum value was 0; other frames were calculated proportionally (Fig. 2). Pulses are defined as smoothed data fragments above the threshold. For apical area constriction pulse, the threshold is 10 µm^2/min. For medial and junctional myosin pulse, the threshold is the average myosin intensity of all cells in each cluster. In Movies 2-5, 7, 8, 11-14, clusters of cells move within the extending germband and tissue drift is corrected with the StackReg plugin in ImageJ for movie display. No tissue drift correction was performed for data quantification and analysis.

Mathematical modeling

A phase-field model was developed to investigate the dynamics of delaminating neuroblasts. In the model, a set of continuous phase-field variables are used, i.e. $\eta_1(x),\eta_2(x),\ldots,\eta_p(x)$, where x is the position and p represents the number of cells in space. Then the shape of the ith cell is described by a narrow transition layer between the interior ($\eta_i(x)$=1) and exterior ($\eta_i(x)$=0) of the cell.

The total free energy is:

$$E_{total} = \int \left[\sum_{i=1}^{p} \frac{\kappa_i}{2} (\nabla \eta_i(x))^2 + f(\eta_1(x), \eta_2(x), \ldots, \eta_p(x)) \right] dx, \quad (1)$$

where the coefficient κ_i is the parameter reflecting the thickness of the cell membrane, and it can also be used to represent the interfacial anisotropy of different types of cells. To simulate the cell-cell interactions, the following free energy density function is used:

$$f(\eta_1(x), \eta_2(x), \ldots, \eta_p(x)) = \sum_{i=1}^{p} \frac{\alpha}{4} \eta_i^2 (\eta_i - 1)^2 + \beta \sum_{i=1}^{p} \sum_{j \neq i}^{p} \eta_i^2 \eta_j^2, \quad (2)$$

where α and β are two parameters of the free energy density function. The general requirement for choosing parameters is that it has p degenerate minima with equal depth, f_{min}, located at: $(\eta_1(x),\eta_2(x),\ldots,\eta_p(x))$=(1,0,…,0), (0,1,…,0),…,(0,0,…,1) in p dimensional space. The last term in Eqn 2 represents the interactions of neighboring cells, such as cell-cell adhesion.

Disregarding cell growth and cell division, the cell area $V=\int \eta(x)dx$ is generally conserved during deformation and movement. So, an apical area constraint term is introduced as follows:

$$E_{area}(\eta_1, \eta_2, \ldots, \eta_p) = \sum_{i=1}^{p} \frac{M}{2} \left(\int \eta_i(x) dx - V_0 \right)^2, \quad (3)$$

where V_0 is the average apical area of each cell. The penalty constant M is defined as $M=M_0\int \eta(x)dx$, so that it allows the cell to delaminate without changing the energy.

Next, the myosin signals are incorporated during the delamination process. Because the molecular origins of cortical forces and the detailed underlying mechanism are uncertain, a phenomenological and simple description of the contraction force caused by the myosin is used:

$$F_{myosin} = -(\rho_M(t) + \lambda \rho_J(t))\vec{n}, \quad (4)$$

where $\vec{n}$ is the unit normal vector on the cell membrane. The total myosin is composed by the medial myosin $\rho_M(t)$ and the junctional myosin $\rho_J(t)$ with a scaling parameter λ. In the simulations, a stochastic medial myosin pulse $\rho_M(t)$ is generated with square wave pulses at regular intervals, with the mean medial myosin intensity as the amplitude and 30 s as the width. For simplification, the junctional myosin $\rho_J(t)$ is selected as a Gaussian random signal as the basal level of the total myosin intensity.

The evolution equations for phase field variables are then governed by:

$$\tau \frac{\partial \eta_i}{\partial t} = -\frac{\delta E_{total}}{\delta \eta_i} - \frac{\delta E_{area}}{\delta \eta_i} + F_{myosin}, \; i = 1, \ldots, p. \quad (5)$$

Here, τ is the relaxation time.

The approximation of the medial myosin pulse $\rho_M(t)$ is estimated by fitting the curve of the distribution of medial myosin intensity for delaminating and nondelaminating cells (Fig. S7). The mean and standard deviation medial myosin intensity for delaminating (0.5027 and 0.2363, respectively) and nondelaminating (0.222 and 0.1712, respectively) cells can then be obtained. The frequency of the medial myosin pulse is 0.8 pulse/min in the delaminating cells and 0.5 pulse/min in the nondelaminating cells (Fig. 2J). The junctional myosin pulse is not significantly different between delaminating cells and nondelaminating cells (Fig. 2N), so the junctional myosin $\rho_J(t)$ is used as a constant for simplification.

In the simulations, the number of cells is selected as six, i.e. p=6. The domain size is 15 µm×15 µm. The period boundary condition is applied and the Fourier spectral method is implemented for space discretization. Some example values of parameters are κ=0.09, M_0=8×10^{-4}, λ=0.1, α=1 and β=1.

The constrained string method (Du and Zhang, 2009) is applied to compute the minimum energy path in Fig. 3A, with 26 images used for discretization of the string in the simulation. The algorithm details of the constrained string method can be found in Du and Zhang (2009).

The semi-implicit scheme for the time discretization is applied to solve Eqn 5 to obtain the simulation in Fig. 4B.

Acknowledgements
We thank Dr Chris Doe for helpful discussion on the project; Dr Adam Martin, Dr Eric Wieschaus, Dr Chris Doe, Dr Bing He, Dr Thomas Lecuit, the Bloomington Drosophila Stock Center and Developmental Studies Hybridoma Bank for providing fly stocks and reagents; Dr Zilong Wen, Dr Karl Herrup and Dr Mingjie Zhang for sharing confocal microscopes; and Dr Trudi Schupbach and Dr Chris Doe for helpful comments on the manuscript.

Competing interests
The authors declare no competing or financial interests.

Author contributions
Conceptualization: Y.Y.; Methodology: Y.A., G.X., L.Z., Y.Y.; Software: X.Z., W.Y.; Validation: Y.A.; Formal analysis: Y.A., G.X., Y.S., D.M., T.I., L.Z.; Investigation: Y.A., L.Z.; Data curation: Y.A., Y.S., D.M.; Writing - original draft: Y.A., L.Z., Y.Y.; Writing - review & editing: Y.A., T.I., Y.Y.; Visualization: Y.A., L.Z.; Supervision: T.I., Y.Y.; Project administration: T.I., Y.Y.; Funding acquisition: T.I., L.Z., Y.Y.

Funding
This work was supported by grants from the Research Grants Council, University Grants Committee of the Hong Kong Special Administrative Region (GRF16103815, 16103314, 16150016, AoE/M-09/12 and ITC-CNERC14SC01 to Y.Y.; GRF16150216 and ECS26100214 to T.I.) and National Natural Science Foundation of China (11622102 and 91430217 to L.Z.).

Supplementary information
Supplementary information available online at
http://dev.biologists.org/lookup/doi/10.1242/dev.150763.supplemental

References
Andersen, P., Uosaki, H., Shenje, L. T. and Kwon, C. (2012). Non-canonical Notch signaling: emerging role and mechanism. *Trends Cell Biol.* **22**, 257-265.
Bertet, C., Sulak, L. and Lecuit, T. (2004). Myosin-dependent junction remodelling controls planar cell intercalation and axis elongation. *Nature* **429**, 667-671.
Blanchard, G. B., Murugesu, S., Adams, R. J., Martinez-Arias, A. and Gorfinkiel, N. (2010). Cytoskeletal dynamics and supracellular organisation of cell shape fluctuations during dorsal closure. *Development* **137**, 2743-2752.
Booth, A. J. R., Blanchard, G. B., Adams, R. J. and Röper, K. (2014). A dynamic microtubule cytoskeleton directs medial actomyosin function during tube formation. *Dev. Cell* **29**, 562-576.
Burgess, D. R. (1982). Reactivation of intestinal epithelial cell brush border motility: ATP-dependent contraction via a terminal web contractile ring. *J. Cell Biol.* **95**, 853-863.
Campos-Ortega, J. A. and Hartenstein, V. (1997). *The Embryonic Development of Drosophila Melanogaster*, 2nd edn. Berlin: Springer.
Campos-Ortega, J. A. and Knust, E. (1990). Genetics of early neurogenesis in Drosophila melanogaster. *Annu. Rev. Genet.* **24**, 387-407.
Coravos, J. S. and Martin, A. C. (2016). Apical sarcomere-like actomyosin contracts nonmuscle drosophila epithelial cells. *Dev. Cell* **39**, 346-358.
David, D. J. V., Tishkina, A. and Harris, T. J. (2010). The PAR complex regulates pulsed actomyosin contractions during amnioserosa apical constriction in Drosophila. *Development* **137**, 1645-1655.
Doe, C. Q. (1992). Molecular markers for identified neuroblasts and ganglion mother cells in the Drosophila central nervous system. *Development* **116**, 855-863.
Du, Q. and Zhang, L. (2009). A constrained string method and its numerical analysis. *Commun. Math. Sci.* **7**, 1039-1051.
Du, Q., Liu, C. and Wang, X. Q. (2004). A phase field approach in the numerical study of the elastic bending energy for vesicle membranes. *J. Comput. Phys.* **198**, 450-468.
Eisenhoffer, G. T., Loftus, P. D., Yoshigi, M., Otsuna, H., Chien, C. B., Morcos, P. A. and Rosenblatt, J. (2012). Crowding induces live cell extrusion to maintain homeostatic cell numbers in epithelia. *Nature* **484**, 546-549.
Gelbart, M. A., He, B., Martin, A. C., Thiberge, S. Y., Wieschaus, E. F. and Kaschube, M. (2012). Volume conservation principle involved in cell lengthening and nucleus movement during tissue morphogenesis. *Proc. Natl. Acad. Sci. USA* **109**, 19298-19303.
Geling, A., Steiner, H., Willem, M., Bally-Cuif, L. and Haass, C. (2002). A gamma-secretase inhibitor blocks Notch signaling in vivo and causes a severe neurogenic phenotype in zebrafish. *EMBO Rep.* **3**, 688-694.
Gu, Y. and Rosenblatt, J. (2012). New emerging roles for epithelial cell extrusion. *Curr. Opin. Cell Biol.* **24**, 865-870.
Hartenstein, V., Younossi-Hartenstein, A. and Lekven, A. (1994). Delamination and division in the Drosophila neurectoderm: spatiotemporal pattern, cytoskeletal dynamics, and common control by neurogenic and segment polarity genes. *Dev. Biol.* **165**, 480-499.
Hava, D., Forster, U., Matsuda, M., Cui, S., Link, B. A., Eichhorst, J., Wiesner, B., Chitnis, A. and Abdelilah-Seyfried, S. (2009). Apical membrane maturation and cellular rosette formation during morphogenesis of the zebrafish lateral line. *J. Cell Sci.* **122**, 687-695.
Hayward, P., Brennan, K., Sanders, P., Balayo, T., DasGupta, R., Perrimon, N. and Martinez Arias, A. (2005). Notch modulates Wnt signalling by associating with Armadillo/beta-catenin and regulating its transcriptional activity. *Development* **132**, 1819-1830.
Hogan, C., Dupré-Crochet, S., Norman, M., Kajita, M., Zimmermann, C., Pelling, A. E., Piddini, E., Baena-Lopez, L. A., Vincent, J. P., Itoh, Y. et al. (2009). Characterization of the interface between normal and transformed epithelial cells. *Nat. Cell Biol.* **11**, 460-467.
Irvine, K. D. and Wieschaus, E. (1994). Cell intercalation during Drosophila germband extension and its regulation by pair-rule segmentation genes. *Development* **120**, 827-841.
Jan, Y. N. and Jan, L. Y. (1994). Neuronal cell fate specification in Drosophila. *Curr. Opin. Neurobiol.* **4**, 8-13.
Kerridge, S., Munjal, A., Philippe, J. M., Jha, A., de las Bayonas, A. G., Saurin, A. J. and Lecuit, T. (2016). Modular activation of Rho1 by GPCR signalling imparts polarized myosin II activation during morphogenesis. *Nat. Cell Biol.* **18**, 261-270.
Kraut, R. and Campos-Ortega, J. A. (1996). Inscuteable, a neural precursor gene of Drosophila, encodes a candidate for a cytoskeleton adaptor protein. *Dev. Biol.* **174**, 65-81.
Kuipers, D., Mehonic, A., Kajita, M., Peter, L., Fujita, Y., Duke, T., Charras, G. and Gale, J. E. (2014). Epithelial repair is a two-stage process driven first by dying cells and then by their neighbours. *J. Cell Sci.* **127**, 1229-1241.
Lecuit, T., Lenne, P. F. and Munro, E. (2011). Force generation, transmission, and integration during cell and tissue morphogenesis. *Annu. Rev. Cell Dev. Biol.* **27**, 157-184.
Marinari, E., Mehonic, A., Curran, S., Gale, J., Duke, T. and Baum, B. (2012). Live-cell delamination counterbalances epithelial growth to limit tissue overcrowding. *Nature* **484**, 542-545.
Martin, A. C. and Goldstein, B. (2014). Apical constriction: themes and variations on a cellular mechanism driving morphogenesis. *Development* **141**, 1987-1998.
Martin, A. C., Kaschube, M. and Wieschaus, E. F. (2009). Pulsed contractions of an actin-myosin network drive apical constriction. *Nature* **457**, 495-499.
Martin, A. C., Gelbart, M., Fernandez-Gonzalez, R., Kaschube, M. and Wieschaus, E. F. (2010). Integration of contractile forces during tissue invagination. *J. Cell Biol.* **188**, 735-749.
Mason, F. M., Tworoger, M. and Martin, A. C. (2013). Apical domain polarization localizes actin-myosin activity to drive ratchet-like apical constriction. *Nat. Cell Biol.* **15**, 926-936.
Mason, F. M., Xie, S., Vasquez, C. G., Tworoger, M. and Martin, A. C. (2016). RhoA GTPase inhibition organizes contraction during epithelial morphogenesis. *J. Cell Biol.* **214**, 603-617.
Munjal, A., Philippe, J. M., Munro, E. and Lecuit, T. (2015). A self-organized biomechanical network drives shape changes during tissue morphogenesis. *Nature* **524**, 351-355.
Rauzi, M., Lenne, P. F. and Lecuit, T. (2010). Planar polarized actomyosin contractile flows control epithelial junction remodelling. *Nature* **468**, 1110-1114.
Röper, K. (2012). Anisotropy of Crumbs and aPKC drives myosin cable assembly during tube formation. *Dev. Cell* **23**, 939-953.

Development (2017) 144, 2153-2164 doi:10.1242/dev.150763

Rosenblatt, J., Raff, M. C. and Cramer, L. P. (2001). An epithelial cell destined for apoptosis signals its neighbors to extrude it by an actin- and myosin-dependent mechanism. *Curr. Biol.* **11**, 1847-1857.

Royou, A., Sullivan, W. and Karess, R. (2002). Cortical recruitment of nonmuscle myosin II in early syncytial Drosophila embryos: its role in nuclear axial expansion and its regulation by Cdc2 activity. *J. Cell Biol.* **158**, 127-137.

Schindelin, J., Arganda-Carreras, I., Frise, E., Kaynig, V., Longair, M., Pietzsch, T., Preibisch, S., Rueden, C., Saalfeld, S., Schmid, B. et al. (2012). Fiji: an open-source platform for biological-image analysis. *Nat. Methods* **9**, 676-682.

Shao, D. Y., Levine, H. and Rappel, W.-J. (2012). Coupling actin flow, adhesion, and morphology in a computational cell motility model. *Proc. Natl. Acad. Sci. USA* **109**, 6851-6856.

Sullivan, W., Ashburner, M. and Hawley, R. S. (2000). *Drosophila Protocols*. Cold Spring Harbor, NY: Cold Spring Harbor Laboratory Press.

Toyama, Y., Peralta, X. G., Wells, A. R., Kiehart, D. P. and Edwards, G. S. (2008). Apoptotic force and tissue dynamics during Drosophila embryogenesis. *Science* **321**, 1683-1686.

Vaccari, T., Lu, H., Kanwar, R., Fortini, M. E. and Bilder, D. (2008). Endosomal entry regulates Notch receptor activation in Drosophila melanogaster. *J. Cell Biol.* **180**, 755-762.

Vasquez, C. G., Tworoger, M. and Martin, A. C. (2014). Dynamic myosin phosphorylation regulates contractile pulses and tissue integrity during epithelial morphogenesis. *J. Cell Biol.* **206**, 435-450.

Wang, W., Tao, K., Wang, J., Yang, G., Ouyang, Q., Wang, Y., Zhang, L. and Liu, F. (2017). Exploring the inhibitory effect of membrane tension on cell polarization. *PLoS Comput. Biol.* **13**, e1005354.

Weng, M. and Wieschaus, E. (2016). Myosin-dependent remodeling of adherens junctions protects junctions from Snail-dependent disassembly. *J. Cell Biol.* **212**, 219-229.